JOM, Vol. 70, No. 7, 2018
https://doi.org/10.1007/s11837-018-2893-1

ADVANCED REAL TIME OPTICAL IMAGING

In Situ Observations of Agglomeration of Non-metallic Inclusions at Steel/Ar and Steel/Slag Interfaces by High-Temperature Confocal Laser Scanning Microscope: A Review

WANGZHONG MU,[1,2] NESLIHAN DOGAN,[1] and KENNETH S. COLEY[1]

1.—McMaster Steel Research Centre, Department of Materials Science and Engineering, McMaster University, 1280 Main Street West, Hamilton, ON L8S 4L7, Canada. 2.—e-mail: wangzhongmu6699@gmail.com

The agglomeration behavior of non-metallic inclusions in the steelmaking process is important for controlling the cleanliness of the steel. In this work, the observation of agglomeration behaviors of inclusions at steel/Ar and steel/slag interfaces using a high-temperature confocal laser scanning microscope (HT-CLSM) is summarized. This HT-CLSM technique has been applied to observe phase transformation during solidification and heat treatment and the engulfment and pushing behavior of inclusions in front of the solidified interface. In the current work, the inclusion agglomeration behavior at steel/Ar and steel/slag interfaces is summarized and discussed. Subsequently, the development of the theoretical work investigating inclusion agglomeration at steel/Ar and steel/slag interfaces including the initial capillary force model and Kralchevsky–Paunov model is described. Finally, the Kralchevsky–Paunov model is applied to investigating nitride inclusion agglomeration at high-manganese steel/Ar interfaces. This work aims to give a critical review of the application of HT-CLSM in secondary refining as well as a better control of inclusion elimination for clean steel production.

INTRODUCTION

The cleanliness of steel is of vital importance in meeting the increasing demands for high-quality steel grades with superior mechanical properties. To improve steel cleanliness, the agglomeration behavior of inclusions in steel must be controlled accurately. Steel plants aim to produce steels with as much cleanliness as possible to avoid nozzle clogging, improve mechanical properties, and ensure economical production.[1–3] Against this background, the field of 'inclusion engineering' has been developed,[4] which deals with control of the morphology, size distribution, amount, and composition of non-metallic inclusions formed in liquid steel during refining and casting processes.

The agglomeration behavior of inclusions has been investigated experimentally by using the high-temperature confocal laser scanning microscope (HT-CLSM). The pioneering work on the application of HT-CLSM dates back to the work of Emi's group,[5,6] with the observation of crystal growth during the solidification of steel[5] as well as engulfment and pushing behaviors of inclusions in steel the melt/solid interface.[6] HT-CLSM has also been used to observe the phase transformations in solid steel during continuous cooling.[7,8] Moreover, previous HT-CLSM work focusing on the observation of inclusion agglomeration behavior at steel/Ar and steel/slag interfaces has been reported in Refs. 9–26.

In the current work, an overview of in situ observation of non-metallic inclusion agglomeration behavior is presented. Furthermore, the theoretical attractive force for inclusion agglomeration was initially calculated by Emi et al.[9,10] and subsequently by Nakajima and Mizoguchi,[11] Kimura et al.,[12] Wikström et al.,[23,26] and Mu et al.[13,14] using the Kralchevsky–Paunov model.[27,28] The calculated results can provide a reasonable fit with the experimental data of attractive force.[11–14,23] Subsequently, the agglomeration potency of different nitride inclusions at a high-manganese steel/Ar interface is quantitatively evaluated, based on the

(Published online May 8, 2018)

calculation results of capillary force. The present work aims to consolidate and rationalize the extensive observations in the literature with the objective of better control of inclusion elimination and improve the steel quality in secondary refining and casting, according to the concept of inclusion engineering.

EXPERIMENTAL WORK OF IN SITU OBSERVATION OF INCLUSION AGGLOMERATION AT STEEL/AR AND STEEL/SLAG INTERFACES BY HT-CLSM

Inclusion Agglomeration at the Steel/Ar Interface

Several researchers have investigated inclusion agglomeration behaviors at steel/Ar[9–22] and steel/slag interfaces[16,19,23–26] by HT-CLSM, as summarized in Table I. Emi et al.[9,10] observed the agglomeration behavior of solid inclusions (Al_2O_3, A80S, CA80S, CAS95, CA80), semi-solid inclusion (CA60), and liquid inclusions (CA60S, CA50S, CA50) at the steel/Ar interface, where CaO is abbreviated as C, Al_2O_3 as A, SiO_2 as S, and MgO as M. The numerals after the abbreviated letters represent the average content in each inclusion, for example, CA60S represents 60 mass%Al_2O_3-xCaO-ySiO_2. They reported that solid–solid inclusion pairs would form as (1) intermediate aggregates, (2) loose structured clusters, and (3) densified compact clusters more easily than other types of inclusion pairs. The attractive capillary force was in the range of 10^{-16}–10^{-13} N. An illustration of the calculation of the attractive force of inclusion agglomeration based on the HT-CLSM video from previous studies[9,10,12] is shown in Fig. 1.

$$a_i = (V_{i+1} - V_i)/\Delta t_i = (d_{i+1}/t_{i+1} - d_i/t_i)\Delta t_i \quad (1)$$

$$\Delta t_i = t_{i+1} - t_i \quad (2)$$

$$m_2 = \rho \times V_2 \quad (3)$$

$$F_{A,i} = m_2 \times a_2 \quad (4)$$

$$F'_{A,i} = m_2 \times a_i \times m_1/(m_1 + m_2) \quad (5)$$

Equations 1–4 show the calculation methods for one inclusion (guest) moving toward a stagnant inclusion (host) where m_1 is the mass of the guest inclusion and a is the acceleration of the guest inclusion toward the host inclusion. Also, d_1, d_2, and d_3 are the distances between two inclusions at each time. The time interval, Δt, equals 1/30 of a second. Furthermore, if two inclusions approach each other, a revised parameter of $m_2/(m_1 + m_2)$ was introduced to replace m_1. In that case, Eq. 5 was introduced. It should be noted that the inclusion is assumed to have a disk shape in Refs. 9, 10 and 12; it is also assumed to have a spherical shape in Refs. 13 and 23. The volume of inclusions can be calculated based on the different geometries.

It is reported that there is no collision between the globular liquid–liquid inclusions. The strength of the attraction force between two inclusions in pairs at the steel/Ar interface can be listed as follows: liquid/liquid pair < liquid/semi-liquid pair < semi-liquid/semi-liquid pair < liquid/solid pair < semi-liquid/solid pair < solid/solid pair.[10] The detailed composition, attractive force, morphology, and agglomeration characteristics of inclusions are summarized in Table II. In addition, Yin et al. claimed that strong long-range attraction extended as far as 50 μm between Al_2O_3 inclusions and about 40 μm between 80%Al_2O_3·20%SiO_2 inclusions.[9]

Subsequently, Nakajima et al.[11,12] continued this research work with reporting data for inclusion agglomeration in 16Cr Al–Si-killed and 16 Cr Si-killed stainless steel.[11] They concluded that an attractive force existed between pairs of inclusions of a similar kind, such as solid/solid, solid/semi-solid. Specifically, the solid/solid inclusion pair had the strongest attraction, and the liquid/liquid inclusion pair had the weakest. However, a repulsive force exists between the complex-liquid inclusion pair. This conclusion is similar but not identical to that reported by Yin et al.[9,10] Subsequently, these researchers claimed that attractive forces between 93%Al_2O_3·7%MgO inclusions and those between MgO inclusions were quite similar in the range of 5×10^{-18}–5×10^{-16} N,[12] approximately 1/10 of the force between Al_2O_3 inclusion pairs reported by Yin et al.[9] The maximum acting length of the force for 93%Al_2O_3·7%MgO inclusion pairs and MgO inclusion pairs was 21–22 μm,[12] which is much shorter than the maximum acting length for Al_2O_3 and 80%Al_2O_3·20%SiO_2. This acting distance is affected by the inclusion size. It is worth noting that the aforementioned 93%Al_2O_3·7%MgO and MgO inclusions, which have a small value of acting distance, had a radius < 5 μm; however, this acting distance can be over 150 μm for Al_2O_3 inclusions with a radius > 40 μm.[13–15]

In situ observations of inclusion agglomeration have been continuously reported in Refs. 16–19 and 23. Some researchers named 'the steel/Ar interface' as 'the molten steel surface,' and these two terms have the same meaning in the HT-CLSM work. Vantilt et al.[17] observed the agglomeration of Al_2O_3·MnO (sol.), Al_2O_3·MnO·SiO_2 (liq.), and Al_2O_3 (sol.) inclusions at the (Mn,Si)-killed steel/Ar interface and found that solid inclusions move freely to form clusters and liquid inclusions are forced to agglomerate, affected by the fluid flow, which is a similar conclusion to that reported by Nakajima et al.[11,12] Also, Coletti et al.[16] reported that the clustering behavior of liquid CaO·Al_2O_3 inclusions (30%CaO·70%Al_2O_3 or 25%CaO·75%Al_2O_3) was not found at the surface of Ca-treated Al-killed low-

Table I. A summary of in situ observations of inclusion agglomeration behavior at the steel/Ar interface and steel/slag interfaces[9–26]

Interface type	Year	Authors	Agglomerated inclusion	Slag system	Steel type (mass%)
Steel/Ar interface	1997	Yin et al.[9,10]	Al_2O_3, Al_2O_3-SiO_2, CaO-Al_2O_3, CaO- Al_2O_3-SiO_2	–	LCAK steel; Fe-3%Si; HSLA steel; Si-killed steel; HC-Ca-treated steel
	2001	Nakajima and Mizoguchi[11]	Al_2O_3-CaO-MgO-SiO_2 system	–	Fe-0.047/0.067% C-16.3%Cr - 0.25/0.6%Mn-0.3%Si-0.0022/0.0048%O (16CrS.S.)
	2001	Kimura et al.[12]	Solid 93% Al_2O_3·7% MgO and MgO	–	Fe-0.04%C-0.02/0.21% Mn (Mg-added Al-killed steel, Mg-killed steel)
	2003	Coletti et al.[16]	CaO-Al_2O_3	–	Fe-0.093%C-1.46%Mn-0.134%Si-0.039%Al-0.00030%O (Ca-treated, Al-killed steels)
	2004	Vantilt et al.[17]	Al_2O_3, Al_2O_3- MnO, Al_2O_3-MnO-SiO_2,	–	Fe-0.047%C-0.64%Mn-0.27%Si-0.006%Al-0.031%Cr-0.006%N (Si–Mn-killed low-C steel)
	2006	Liang et al.[18]	CaO-MgO- Al_2O_3-SiO_2	–	Fe-17%Cr-8.36%Ni-0.06%C-0.63%Si-0.7%Mn (AISI 304 S.S.)
	2008	Appelberg et al.[19]	Al_2O_3·Ce_2O_3	–	79 ~ 80% Fe-19 ~ 20% Cr- 0.1%Al-(0.002 ~ 0.1)%Ce
	2008	Wikström et al.[23]	Al_2O_3-CaO	–	Fe-0.75%C-0.18Si-0.48%Mn-0.001%Al-0.0012%Ca-0.01%Cu-0.003%O (HC-Ca-treated steel), the same composition as in Ref. 8
	2011	Kang et al.[20]	Al_2O_3, MgO·Al_2O_3, CaO·2Al_2O_3, liquid inclusion	–	Fe-0.39%C-1.0%Si-0.4%Mn-5.3%Cr-1.3%Mo-0.9%V
	2016	Du et al.[21]	Al_2O_3, MgO·Al_2O_3	–	Fe-0.4%C-1.0%Si-0.3%Mn-5%Cr-1.2%Mo-0.9%V-0.14%Ni-0.017/0.024%Al-0/0.001%Mg
	2016	Michellic et al.[22]	CaO·xAl_2O_3 (CAx)	–	Fe-0.15%C-0.02%Si-1.07%Mn-0.04%Al-0.002%Ca-0.004%S
	2017	Mu et al.[13–15]	Al_2O_3 containing trace Ti oxide	–	Fe-0.16%C-0.84%Mn-0.15%Si-0.008%Ti-0.01%Al-0.03%S
Steel/slag interface	2000	Misra et al.[24]	Al_2O_3·CaO·SiO_2	50% CaO-50% Al_2O_3	Fe-1.3%Si-1.1%Mn-1.2%Al
	2001	Misra et al.[25]	TiN	39.5%SiO_2-33.4%CaO-19.5%Al_2O_3-7.3% MgO	85.4%Fe -13.52%Cr -0.17%Ti-0.23%Ni-0.16% Al- 0.39%Si -0.11%Ca
	2003	Coletti et al.[16]	Al_2O_3,Al_2O_3-SiO_2-containing inclusion	C55.3A46.5S0.1, C40A20S40, C33A20S40Mg7	Fe-0.093%C-1.46%Mn-0.134%Si-0.039%Al-0.00030%O (Ca-treated, Al-killed steels)
	2004	Vantilt et al.[17]	Al_2O_3-CaO-MnO-SiO_2	C50A50, C40A20S40, C55.3A46.5S0.1, C33A20S40Mg7	Fe-0.047%C-0.64%Mn-0.27%Si-0.006%Al-0.031%Cr-0.006%N [(Si–Mn)-killed LC steel]
	2008	Wikström et al.[23,26]	Liquid CaO- Al_2O_3	20.7%Al_2O_3-36.5% CaO-42.8%SiO_2	Fe-0.75%C-0.18%Si-0.48%Mn-0.001%Al-0.0012%Ca-0.01%Cu-0.003%O (HC-Ca-treated steel)

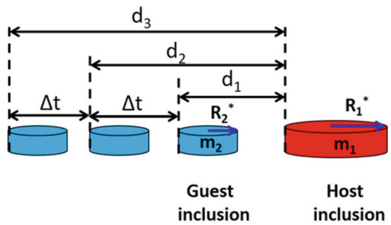

Fig. 1. Schematic illustration to calculate the attractive force from the HT-CLSM video, adapted from Refs. 9, 10, and 12.

carbon steel.[16] Similar phenomena regarding the motion of complex Al_2O_3·SiO_2·CaO·MgO inclusions at the molten steel surface and the δ-ferrite/liquid interface of AISI 304 stainless steel were reported by Liang et al.[18] Appelberg et al.[19] reported the agglomeration behavior of alumina and cerium oxide (Al_2O_3·Ce_2O_3) inclusions in liquid Fe-20%Cr ferric stainless steel. Different types of alumina and cerium oxide inclusions have been observed according to the different ratios of [Ce]/[Al] in the steel. However, all the types of Al_2O_3·Ce_2O_3 inclusions could form clusters with radii up to approximately 20 μm.[19] Wikström et al.[23] reported the agglomeration behavior of two types of Ca–Al oxides, liquid 50%Al_2O_3·50%CaO (CA50) and semi-liquid 62%Al_2O_3·38%CaO (C38A62) inclusions, at the surface of high-carbon Al-killed steel with Ca treatment. They claimed that the collide type between the semi-liquid C38A62 inclusion pair was 'free' and that between the liquid–liquid CA50 inclusions was both 'free' and 'forced.' This conclusion means that the liquid–liquid inclusion pair could not collide as freely as the liquid/semi-liquid inclusion pair, which is similar to the conclusion reported in previous studies.[9–12] However, the liquid–liquid inclusion pair can be forced to agglomerate at the steel/Ar interface, driven by the steel flow when the temperature increases. Besides, MgO·Al_2O_3 is a technologically important inclusion type, which may lead to nozzle clogging. Regarding this type of inclusion, Kang et al.[20] reported that Al_2O_3 inclusions attracted each other and agglomerated. However, MgO·Al_2O_3 spinel inclusions and solid calcium aluminate inclusions did not show any sign of attraction or agglomeration. Du et al.[21] reported Al_2O_3 and MgO·Al_2O_3 spinel behaviors in Fe-0.4C-1Si-0.3Mn-5Cr-1.2Mo-0.9V Al-killed steels with and without Mg addition. They observed agglomerated MgO·Al_2O_3 spinel clusters of 20–60 μm; however, their number and size were much smaller than the Al_2O_3 clusters in the same steel grade without Mg addition. To date, the exact reason for the different agglomeration behaviors of MgO·Al_2O_3 spinel inclusions reported by different researchers[20,21] is unclear; it may be related to the different physical properties of various steel grades or the number density of the MgO·Al_2O_3 spinel inclusions presented in the steels.

Inclusion Agglomeration Behavior at the Steel/Slag Interface

The use of HT-CLSM to investigate the inclusion agglomeration behavior at the steel/slag interface dates back to the work of Sridhar's group.[16,17,24,25] A schematic illustration of the steel/Ar and steel/slag interfaces before in situ observation experiments is shown in Fig. 2. To observe the inclusion agglomeration behavior at the steel/slag interface, an optically transparent slag disc should be used.[16,17,23,26] Another required condition is the melting point of the slag should be lower than that of the steel. According to these two requirements, a 50% CaO·50% Al_2O_3 slag[16,23] and several CAS slags with or without MgO[19,24–26] were selected in previous studies.

Detailed information on the agglomeration behavior of inclusions at the steel/slag interface is shown in Table I. Misra et al.[24] reported the agglomeration behavior of different types of Al_2O_3·CaO·SiO_2 inclusions at the interface created by a (Mn,Si)-killed steel and a 50%CaO·50%Al_2O_3 slag. Irregular inclusions (solid) with sizes < 10 μm would occasionally attract and absorb irregular inclusions with smaller size to form aggregates. This qualitative observation is quite similar to the case of inclusion behavior at the steel/Ar interface.[9–11] Thereafter, the agglomeration of different morphologies of TiN inclusions at a molten stainless steel/CASM slag interface was reported by the same authors.[25] Loose clusters with hexagonal-shaped TiN precipitates could be observed at 1489°C. However, triangular-shaped TiN precipitates were found to form clusters at 1589°C.[25]

Quantitative analysis of the attractive force of inclusion agglomeration at the steel/slag interface has been continuously reported.[16,17,23,26] Coletti et al.[16] and Vantilt et al.[17] reported that the same types of 40%CaO·40%SiO_2·20%Al_2O_3, 53.3%CaO·46.5% Al_2O_3·0.1%SiO_2, and 33%CaO·20%Al_2O_3·40%SiO_2·6 7%MgO slags were used to create the steel/slag interface. Moreover, (Mn,Si)-killed low-carbon steel,[17] abbreviated as LC-SMn steel, and Ca-treated Al-killed low-carbon steel,[16] abbreviated as LC-CA steel, were chosen. For the case of LC-SMn steel, complex liquid Al_2O_3·CaO·MnO·SiO_2 inclusions were found, and the agglomeration of this type of inclusion was reported to be inhibited by a counteracting force at the steel/slag interface. This differs from the behavior of similar types of inclusions at the steel/Ar interface, where solid inclusions (Al_2O_3 and Al_2O_3·MnO) were observed to move freely to form a cluster, and liquid inclusions (Al_2O_3·MnO·SiO_2) were forced to agglomerate under the influence of fluid flow.[17] For the case of LC-CA steel, the inclusion is identified as the solid Al_2O_3 and Al_2O_3-SiO_2-containing phase.[16] Wikström et al.[23,26] reported the clustering behavior of liquid Al_2O_3·CaO inclusions at the interface between

Table II. The summary of composition, morphology, agglomeration characteristics, and attractive force of inclusions observed at the steel/Ar interface in previous studies[9–12,18,19]

Inclusion	Composition (mass%) CaO	Al_2O_3	SiO_2	MgO/Ce_2O_3	State in liq. steel	Shape	Radius (μm)	Attractive force (N)	Initial product of collision	Steel type	Refer -ences
Al_2O_3	–	100	–	–	Solid	Irregular with tips	~2	1.8E−15	Loose cluster	LCAK	9
A80S	–	> 2000980	< 20	–	Solid	Irregular with smooth surface	1 ~ 3	7E− 16	Dense cluster	Fe-3%Si	9
CA60S	> 30	~60	< 10	–	Liquid	Globular	5 ~ 10	–	No collision	HSLA	10
C30A60M10	~32	~61	0	~7 (MgO)	Sol.–Liq.	Globular with tips	1.5 ~ 15.5	1E− 14 ~ 1E− 17	Collision	16Cr Al–Si killed	11
CA80S	< 10	75 ~ 90	10 ~ 20	–	Solid	Irregular with smooth surface	1 ~ 3	4E− 16	Dense cluster	Si-killed steel	10
CAS95	< 5	< 2	> 95	–	Solid	Near globular with hard surface	5 ~ 10	8.2E− 15	Coarse cluster		
CA50S	20 ~ 30	40 ~ 60	20 ~ 30	–	Liquid	Globular	5 ~ 10	–	No collision		
C8A92	7 ~ 9	91 ~ 92	< 1	< 1 (MgO)	Solid	Irregular	2.5 ~ 25	1E− 14 ~ 1E− 18	Collision	16 Cr Si-killed	11
CA80	< 20	> 80	–	–	Solid	Irregular with coarse tips	3 ~ 5	6.5E− 14	Coarse cluster	HC-Ca	10
CA60	30 ~ 35	60 ~ 65	–	–	Sol.- liq.	Irregular with coarse tips	5 ~ 10	1E− 16	Larger globular		
CA50	40 ~ 60	40 ~ 60	–	–	Liquid	Globular	5 ~ 10	–	No collision		
	44 ~ 55	45 ~ 56	–	–	Liquid	Globular	10 ~ 40	–	Forced collision		19
C40A55M5	38 ~ 45	48 ~ 55	< 1	5 ~ 7 (MgO)	Liquid	Globular	< 40	No value	Cluster	AISI 304 S.S.	11
A93M7	–	93	–	7 (MgO)	Solid	–	–	5E− 18 ~ 5E− 16	Coagulation, weaker than Al_2O_3	LCAK	12
MgO	–	–	–	100	Solid	–	–			LCMK	12
$Al_2O_3{\cdot}Ce_2O_3$	–	> 79	–	< 21 (Ce_2O_3)	Sol.-liq.	Semi-globular and irregular	1 ~ 9	No exact value	Cluster	Fe-20%Cr S.S.	18
	–	20 ~ 70	–	55 ~ 80 (Ce_2O_3)	Solid	Irregular, some with tips	1 ~ 11		Cluster	Fe-20%Cr S.S.	18
	–	< 15	–	> 85 (Ce_2O_3)	Sol.-liq.	Semi-globular and irregular	1 ~ 10		Cluster	Fe-20%Cr S.S.	18

CaO is abbreviated as C, Al_2O_3 as A, SiO_2 as S, and MgO as M.Low-carbon Al-killed steel is abbreviated as LCAK, low-carbon Mg-killed steel as LCMgK, stainless steel as S.S., high-strength low-alloy steel as HSLA, and high-carbon Al-killed with Ca-treated steel as HC-Ca.

Ca-treated Al-killed high-carbon steel, abbreviated as HC-CA steel, and the 40%CaO·20%Al_2O_3·40%-SiO_2 slag.

Even if the steel compositions are different, several conclusions are still in agreement. First, the steel would form a pronounced meniscus, penetrating into the slag. A schematic illustration is shown in Fig. 3. The inclusions could be driven together at the top of the hemispherical meniscus because of the buoyancy force. Second, there is an attractive force working at relatively long distances between inclusions or clusters to force them to converge. Thereafter, a repulsive force seems to exist holding back inclusions when they approach within about 150 μm. However, the repulsive force is quite weak, and the inclusions will finally agglomerate at the steel/slag interface.[16,17] Coletti et al.[16] and Vantilt et al.[17] reported the repulsive force could be observed at the interface between low-carbon steel and 33%CaO·20%Al_2O_3·40%SiO_2·6 7%MgO slag; see Fig. 4a. More specifically, Fig. 4b indicates that the repulsive force is larger when the size of the approaching inclusion is larger.[17] According to these authors' understanding, whether the force is attractive or repulsive depends on the wetting behavior between the inclusion and the liquid steel and between the inclusion and slag at the interface.

In the original Refs. 16 and 17, the repulsive force was defined as positive and the attractive force as negative. In this article, the attractive force is defined as positive and the repulsive force as negative; see Fig. 4b. The value of the repulsive force is in the range of 1E−17 to 1E−16 N, which is quite weak. In this case, the inclusions can finally agglomerate, driven by the slag flow forces. Experimental evidence is shown in Fig. 5. It is found that the distance between inclusions decreases with prolonged time. Moreover, Wikström et al.[23,26] reported a similar phenomenon at the interface between HC-CA steel and 40%CaO-20%Al_2O_3-40%SiO_2 slag. Figure 6 shows the distance between pairs of liquid 50%CaO·50%Al_2O_3 inclusions as a function of time. For convenience, each individual inclusion is labeled I, II, and III, the resulting pairs being I and II, I and III, and II and III. The free attraction behavior can be seen between 0 s and 4.5 s for inclusions I and II. Thereafter, the inclusions reach a neutral position until 16 s. After this, the liquid inclusions are forced together by the slag flow forces, as observed by Wikström et al.[23] For the

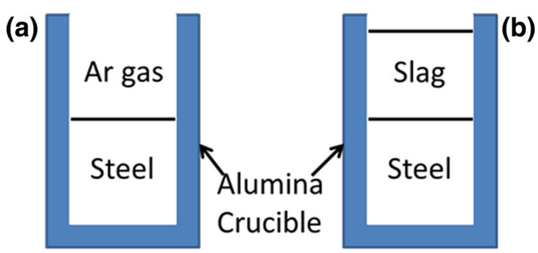

Fig. 2. Schematic illustrations of the (a) steel/Ar and (b) steel/slag interfaces, which were prepared before in situ observation, adapted from Ref. 23.

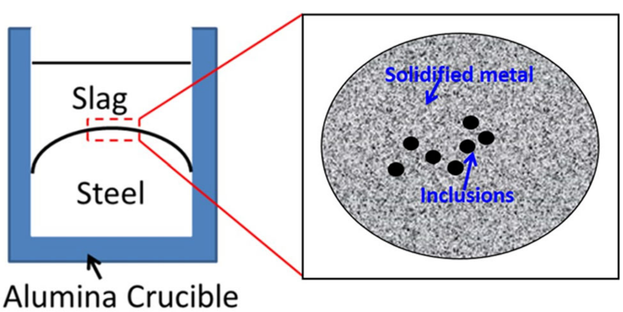

Fig. 3. Illustration of the steel/slag interface after the HT-CLSM experiment, adapted from Ref. 17.

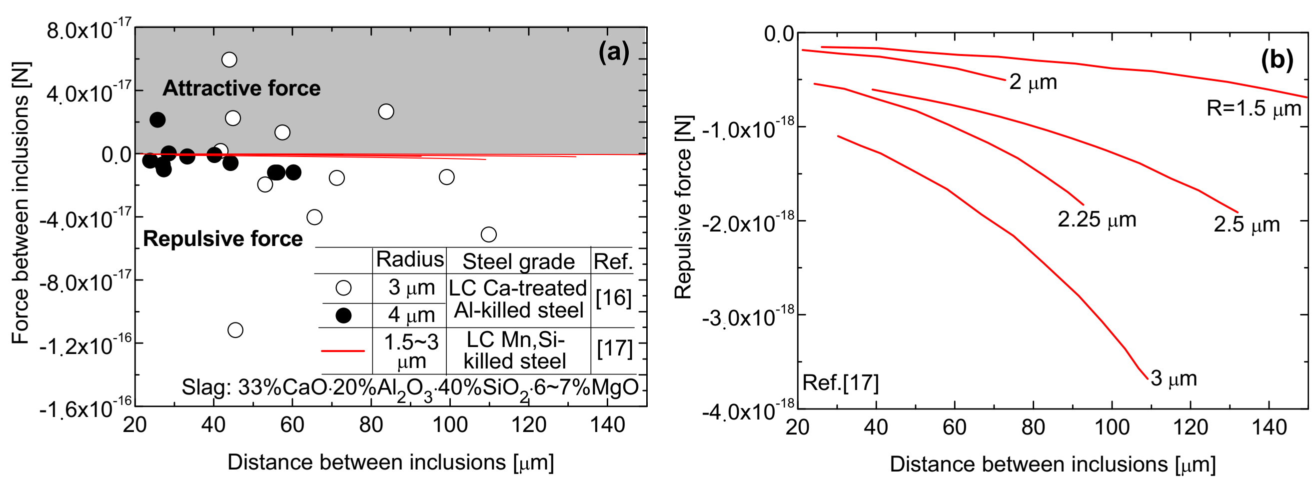

Fig. 4. Comparison of the attractive force and repulsive force between the inclusion and cluster in the low-carbon steel/33%CaO·20%Al_2O_3·40%SiO_2·6 ∼ 7%MgO slag interfaces.

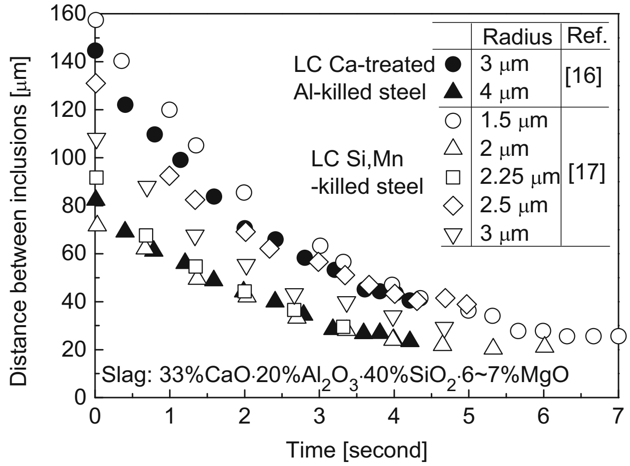

Fig. 5. Comparison of distance between inclusions at the interfaces between LC-CA and LC-SMn steels and 33%CaO·20% Al_2O_3·40% SiO_2·6 ~ 7%MgO slag.

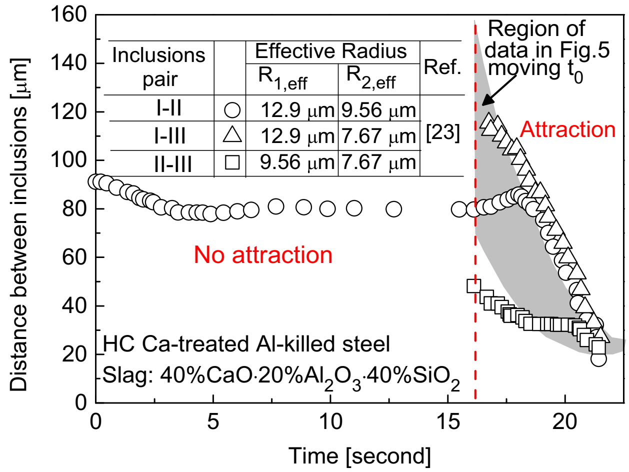

Fig. 6. Comparison of distance between inclusions at the interfaces between HC-CA steel and 40%CaO·20%Al_2O_3·40% SiO_2 slag.

other pairs of inclusions, I-III and II-III, the forced agglomeration is directly observed. By adjusting the starting time of the inclusion agglomeration in Fig. 5 to be the same as for inclusion pairs I-III and II-III, the agglomeration in Fig. 5 can also be considered the forced type because of the overlapping data. It should be noted that the term 'forced agglomeration' is used in Refs. 23 and 26, but not in the Refs. 16 and 17. Finally, the inclusion compositions were reported to change because of the reaction between the inclusion and the slag; however, no comment was made regarding the effect of this change.

Summary of In Situ Observation Experiments of Inclusion Agglomeration by HT-CLSM

In situ observations of inclusion agglomeration at the steel/Ar interface can be summarized as follows: Pairs of inclusions of like phases exhibit attraction, and the solid/solid pair shows the strongest attraction followed by the semi-liquid/semi-liquid pair and liquid/liquid pair. For the case of inclusion pairs with different phases, both an attractive force and a repulsive force exist. The difference depends on the physical properties, especially the contact angle between the inclusion and the liquid steel. For the inclusion agglomeration at the steel/slag interface, the force is more complicated. There is a long-distance-range attractive force and a repulsive force when the spacing is < 100–150 μm. Inclusions at the steel/slag interface can be forced to agglomerate by the slag flow.[23] The range of distance for different inclusion agglomerations at the steel/slag interface is different, but no explanation for this has been offered. This issue is worthy of detailed investigation in future work.

Besides the case of the steel/Ar and steel/slag interfaces, the inclusion agglomeration behavior in slag was reported by Wikström et al.[23] as well, and they claimed that the agglomeration of liquid inclusions was enhanced remarkably compared with inclusion agglomeration behavior at the steel/slag interface. However, dissolution of inclusions in the slag was not observed by these researchers. This may be due to the inclusion time because the inclusion in the slag is too short for observation. Lee et al.,[29] Miao et al.,[30] Monaghan et al.,[31–33] and Feichtinger et al.[34] observed various inclusions dissolved in the slag after it transferred across the steel/slag interface by using CLSM. The more systematic in situ observation work in combination with the inclusion agglomeration and dissolution in liquid slag can be considered in future work.

According to previous studies, the agglomeration behavior of Al_2O_3, Al_2O_3·SiO_2, different types of Al_2O_3·CaO, MgO, Al_2O_3·MgO, Al_2O_3·Ce_2O_3, and complex inclusions containing Al, Si, Ca in low-/high-carbon steels, and specific grades of stainless steels (AISI304, 16Cr) have been reported. However, the agglomeration behavior of other types of inclusions, such as Ti oxides and Ti–Al spinel, has not been reported extensively. Moreover, inclusion agglomeration behaviors in other kinds of high-alloy steels, for instance, high-manganese steel, have not been found in the open literature. In addition, physical property data, especially the contact angle for inclusions at the steel/Ar and steel/slag interfaces, are required to calculate the interaction force.

THEORETICAL STUDY OF INCLUSION AGGLOMERATION AT THE STEEL/AR AND STEEL/SLAG INTERFACES

To compare with the experimental evidence of inclusion agglomeration at the steel/Ar and steel/slag interfaces observed by HT-CLSM, a theoretical study on summarizing the calculation methods of the attractive capillary force is introduced in this section. Subsequently, the coagulation coefficients for inclusion agglomeration as well as the

Kralchevsky–Paunov model applied in high-manganese steel melts are calculated. The hybrid calculations, combining attractive capillary force and the coagulation coefficient, aim to give a quantitative comparison of the agglomeration/dispersion potencies of different inclusions in the steels.

Initial Theoretical Attractive Force Model

Yin et al.[9,10] were the first to report that the difference of capillary pressure between the inside and outside of the inclusion pair can push the two inclusions toward each other when they are sufficiently closed; this is called capillary attraction. At that time, a quantitative model to calculate the capillary force between two inclusions at the steel/Ar interface had not been developed, and Eqs. 6 and 7 were used as a preliminary estimation for the capillary force calculation.

$$F = 0.5g \times (\rho_L - \rho_G) \times w \times \Delta h^2 \quad (6)$$

$$\Delta h = 2\gamma \times \cos\theta / g \times (\rho_L - \rho_G) \times \delta \quad (7)$$

where Δh is the difference in the liquid surface height between the inside and outside of the inclusions, w is the width of the surface roughness of the particles, θ is the contact angle between the inclusion and liquid metal, γ is the surface tension, δ is the separation distance, and ρ_L and ρ_G are the densities of the liquid metal and the gas; however, ρ_G is always negligible.

This model gives the first method to evaluate the capillary force for inclusion agglomeration; however, it does not work properly. For instance, it is reported that Δh is calculated to be 0.6 m if using 50 μm of δ, 7000 kg/m^3 of ρ_L, 1.54 N/m of γ, 133° of θ, and 1.25 of surface roughness of Al_2O_3. To get a reasonable capillary force (3.5×10^{-14} N), 0.32 μm of Δh is estimated.[9] In this case, the model does not provide a reasonable evaluation of the attraction capillary force of different inclusions. To calculate the capillary force more accurately, the Kralchevsky–Paunov model was introduced.[27,28]

Kralchevsky–Paunov model

According to the calculation of the attractive capillary force, Kralchevsky et al.[27] derived a general mathematical model for the energy and force balances between two spherical particles floating on the surface of a liquid phase, and this model is used at room temperature. Subsequently, Paunov et al.[28] provided simplified equations to calculate the capillary interaction between the two floating particles at the interface between liquid metal and Ar. Nakajima et al.[11,12] were the first to apply this model to process metallurgy, calculating the capillary force for inclusion agglomeration at the liquid steel/Ar interface. However, the inclusions in the calculation are only defined as solid, liquid, and complex particles. The quantitative analysis for specific kinds of inclusion was not made. Subsequently, Mu et al.[13,14] applied this model to compare with experimental data from in situ observation of large Al_2O_3 inclusions containing minor Ti-oxide inclusions, and reasonable agreement was obtained. Based on the agreement, parametric studies on the effects on the capillary force, inclusion size, surface tension of metal, inclusion density, and contact angle between the inclusion and metal were carried out, and finally the order of the capillary force for a range of oxides (Ce_2O_3, Al_2O_3, Ti_2O_3, MgO, CaO, TiO_2, SiO_2, different spinel oxides) at the interface between Ar and pure iron and medium carbon steel was evaluated quantitatively. In addition, this model has been applied in the in situ dynamic study of the bending deformation of an Al_2O_3 chain aggregate. It was concluded that the capillary force between two particles in an Al_2O_3 chain aggregate is the main driving force for the aggregate bending at the steel/Ar interface.[15] The main equations for the model derivation are summarized here, and the details can also be found elsewhere.[11–14] Figure 7 shows the schematic illustration of the interaction force existing on a pair of spherical particles with radii R_1 and R_2 floating at the steel/Ar interface.

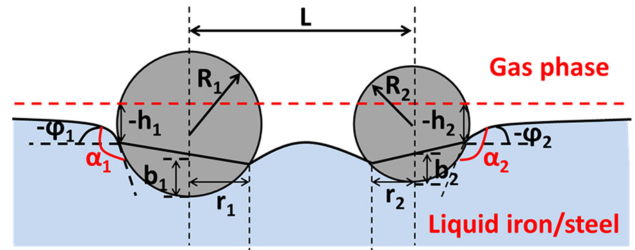

Fig. 7. Schematic illustration of the capillary meniscus around two spherical inclusions at the steel/Ar interface.

Equation 8 shows the capillary interaction energy, W, between spherical inclusions.

$$\Delta W = -\pi\gamma \sum_{k=1}^{2} (Q_k h_k - Q_{k\infty} h_{k\infty})(1 + O(q^2 R_k^2)) \quad (8)$$

$$q = \sqrt{\frac{(\rho_{\mathrm{I}} - \rho_{\mathrm{II}})g}{\gamma}} \approx \sqrt{\frac{\rho_{\mathrm{I}} g}{\gamma}}, \quad \text{where } \rho_I \gg \rho_{II} \quad (9)$$

where ρ_{I} and ρ_{II} are the densities of liquid iron/steel(I) and Ar(II). q is the capillary length, defined by Eq. 9. g is acceleration due to gravity. γ is the surface tension of the liquid metal. The subscript k represents inclusion 1 or 2 in a pair. $O(x)$ is the zero function of the approximation. Subsequently, the capillary charges and height differences of the meniscus (Q_k and $Q_{k\infty}$, and h_k and $h_{k\infty}$) can be calculated using the following equations.

$$Q_k = \frac{1}{2} q^2 b_k^2 \left(R_k - \frac{1}{3} b_k\right) - \frac{4}{3} D_k R_k^3 - r_k^3 h_k \quad (10)$$

$$h_k = (\tau_k + 2\ln(1-\exp(-2\tau_k))) - (Q_1+Q_2)\ln(\gamma_e qa) + (Q_1-Q_2)\left(A - (-1)^k \sum_{n=1}^{\infty} \frac{2}{n}\frac{\exp(-n\tau_k)\sinh n\tau_j}{\sinh n(\tau_1+\tau_2)}\right) \quad (11)$$

where j and $k = 1$ and 2 and $j \neq k$; $(qR_k)^2 \ll 1$. According to Fig. 7, R_k is the radius of inclusion k, b_k is the immersion depth, r_k is the capillary meniscus radius, ϕ is the angle according to the slope of the meniscus, α_k is the contact angle between the inclusion and the liquid metal at the steel/Ar interface, and L is the distance between the inclusions at the interface. γ_e is the Euler–Masceroni constant and is reported to equal 1.78.[11,12,23] D_k is the density ratio. The parameters A, τ_k, and a are used for the simplification of Eq. 11. The calculation of each parameter described above can be seen in Eqs. 12–17.

$$A = \sum_{n=1}^{\infty} \frac{1}{n}\frac{\sinh n(\tau_1-\tau_2)}{\sinh n(\tau_1+\tau_2)} \quad (12)$$

$$\tau_k = \ln\left(\frac{a}{r_k} + \left(\frac{a^2}{r^2}+1\right)^{0.5}\right) \quad (13)$$

$$a^2 = \left(L^2-(r_1+r_2)^2\right)\left(L^2-(r_1-r_2)^2\right)/(2L)^2 \quad (14)$$

$$D_k = R_k(1+\cos(\alpha_k+\varphi_k)) \quad (15)$$

$$\varphi_k = \mathrm{arc}\ \sin(Q_k/r_k) \quad (16)$$

$$r_k = 0.5\left(R_k\sin\alpha_k + (R_k^2\sin^2\alpha_k + 4Q_kR_k\cos\alpha_k)^{1/2}\right) \quad (17)$$

Equation 11 can be simplified as Eq. 18 for the case of agglomeration of two inclusions with the same composition and size.

$$h'_k = Q_k(\tau_k + 2\ln(1-\exp(-2\tau_k))) - (Q_1+Q_2)\ln(\gamma_e qa) \quad (18)$$

When L approaches ∞, $Q_{k\infty}$ and $h_{k\infty}$ become Eqs. 19 and 20.

$$Q_{k\infty} = \frac{1}{6}q^2R_k^3(2-4D_k+3\cos\alpha_k - \cos^3\alpha_k) \quad (19)$$

$$h_{k\infty} = r_{k\infty}\sin\alpha_k\varphi_{k\infty}\frac{4}{\gamma_e q(1+\cos\varphi_{k\infty})} \quad (20)$$

For the different values of L, the capillary force can be calculated as follows.

$$F = \frac{d(\Delta W)}{dL} \quad (21)$$

Here, the capillary interaction energy between two inclusion particles (ΔW) is expressed by the wetting contribution (ΔW_w), meniscus surface tension contribution (ΔW_m), and gravity contribution (ΔW_g); see Eqs. 22–24. The detailed derivation has been reported by Kralchevsky and Paunov.[27,28]

$$\frac{d\Delta W_w}{dL} = -\pi\gamma\sum_{k=1}^{2}(qr_k)^2R_k\cos\alpha_k\frac{dh_k}{dL}\times\left[1+O(q^2R_k^2)\right] \quad (22)$$

$$\frac{d\Delta W_m}{dL} = \pi\gamma\sum_{k=1}^{2}\left[Q_k+(qr_k)^2R_k\cos\alpha_k\right]\frac{dh_k}{dL}\times\left[1+O(q^2R_k^2)\right] \quad (23)$$

$$\frac{d\Delta W_g}{dL} = -\pi\gamma\sum_{k=1}^{2}2Q_k\frac{dh_k}{dL}\left[1+O(q^2R_k^2)\right] \quad (24)$$

$$F = -\pi\gamma\sum_{k=1}^{2}Q_k\frac{dh_k}{dL}\left[1+O(q^2R_k^2)\right] \quad (25)$$

Here, a simplification has been made by Paunov et al.[28] The following Eq. 26 has been used.

$$h_k = h_{k\infty} + Q_jK_0(qL) \quad (j,k = 1,2; j\neq k; r_k \ll L) \quad (26)$$

where the function $K_0(x)$ represents the modified Bessel function of zero order.[35]

By substituting Eq. 26 into Eq. 25, the expression of Eq. 27 can be obtained.

$$F = 2\pi Q_1Q_2qK_1(qL)\left[1+O(q^2R_k^2)\right] \quad (r_k \ll L) \quad (27)$$

where $K_1(x)$ is the modified Bessel function of the first order, and its analogous formula can be seen in Eq. 28.[35,36]

$$K_1(x) = \frac{1}{x} + O(x\ln x) \quad (x\to 0) \quad (28)$$

By substituting Eq. 28 into Eq. 26, the simplification of the attractive capillary force calculation has been made. Paunov et al.[28] reported the final simplified equation can be expressed as Eq. 29; more details can be found in Ref. 28. This equation is made when the distance between two particles, L, is between r_k and q^{-1}.

$$F = 2\pi\gamma\frac{Q_1Q_2}{L} \quad (r_k \ll L \ll q^{-1}) \quad (29)$$

$$O(x\ln x) \approx 0 \quad (x\to 0) \quad (30)$$

Here, the assumption defined by Eq. 30 has been used in Ref. 28. Even if this is not directly reported, this assumption can be judged from expression of Eq. 29.

Mu et al.[13] reported a revised approximation according to the L'Hôpital's rule,[37] and the expression of the capillary force can be seen in Eq. 31, which is the most recently developed equation to calculate the capillary force for inclusion agglomeration at the steel/Ar interface.

$$F = \frac{2\pi Q_1 Q_2 (1 - q^2 L^2)}{L} \quad (r_k \ll L) \quad (31)$$

Application of the Capillary Force Model for Inclusion Agglomeration at the Interface Between Ar and High-Manganese Steel

The above-mentioned Kralchevsky–Paunov capillary force model has been applied to calculate inclusion agglomeration in pure iron and medium carbon steel.[13,14] The agglomeration tendency of different inclusions at the pure iron/Ar and medium carbon steel/Ar interfaces seems to be similar because of the similarity in the physical properties of pure iron and medium carbon steel, including the surface tension, density of liquid metal, and contact angle and interfacial energy between inclusion and liquid metal. Here, the capillary force model is applied to calculate the inclusion agglomeration behavior in high-alloy steel, and thus the agglomeration of nitride inclusions at the interface between Ar and high-manganese steel is discussed in this section, since nitride inclusions can be formed in the liquid state of high-manganese steel, whereas generally nitrides only precipitate in solid-state low-alloy steel. Specifically, AlN has been observed to be one of the major inclusion types in solidified high-manganese TWIP steel (Fe-16.83%Mn-0.58%C-2.1%Al-0.0041%N).[38] Moreover, equilibrium calculations show that AlN can form in the liquid state in high-manganese steel.[39] Park et al. reported the morphology of agglomerated AlN inclusions.[40] Also, Kikuchi et al.[41] claimed the existence of TiN in low-carbon high-manganese steel. In this case, the attractive capillary forces and coagulation coefficient representing the inclusion agglomeration potency in the liquid metal matrix of AlN and TiN are calculated, and the obtained results are shown in Figs. 8 and 9. The physical parameters used for this calculation were collected from the published literature[42–47] and are summarized in Table III. The calculation method of coagulation coefficient can be seen in Ref. 14. TiN was found to agglomerate more readily than AlN, and the calculation result of attractive capillary forces is in agreement with the result of the coagulation coefficient. The agglomeration behavior of oxide inclusions in high-manganese steel cannot be quantitatively discussed, because the relevant physical properties are not available in the open literature, which can be considered in future work.

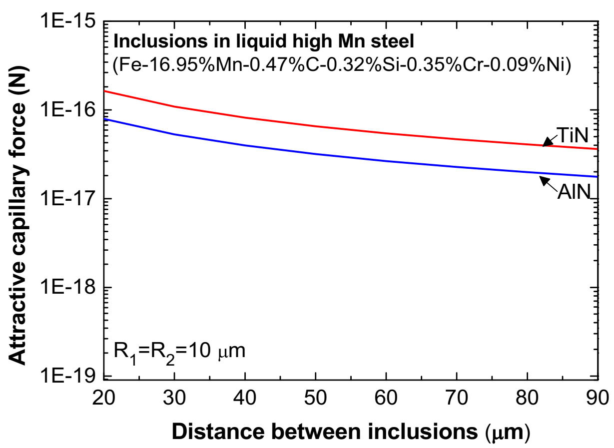

Fig. 8. Comparison of the attractive capillary force of TiN and AlN at the interface between Ar and high manganese steel.

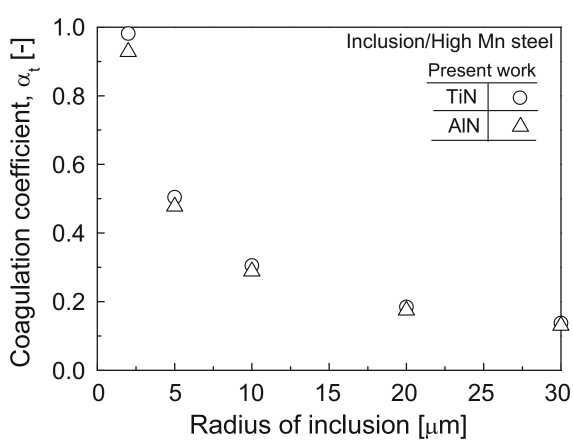

Fig. 9. Comparison of coagulation coefficient of different TiN and AlN in high manganese steel matrix.

SUMMARY

High-temperature confocal laser scanning microscope (HT-CLSM) is an effective technique to observe inclusion agglomeration in situ at steel/Ar and steel/slag interfaces. Previous studies focusing on this topic have been summarized in this article. The HT-CLSM methodology can be applied in a comprehensive study of the behaviors of various

Table III. Physical parameters used for the calculation of the capillary attractive force and the coagulation coefficient of inclusions in high-manganese steel[42–47]

Inclusion	ρ_1 (kg/m^3)	ρ_2 (kg/m^3)	α_1(°)	α_2 (°)	ρ_{iron} (kg/m^3)	γ_M (J/m^2)	γ_I (J/m^2)	γ_{IM} (J/m^2)
TiN	5400	5400	123	123	6600	1.686	1.29	2.221
AlN	3260	3260	132	132	6600	1.304	0.88	1.768

types of inclusions at different steel/Ar and steel/slag interfaces in the future work. Besides experimental work, a modified agglomeration model previously proposed by the current authors is also used to calculate the agglomeration behavior of nitride inclusions at the high-manganese steel/Ar interface, and the result shows that TiN agglomerates more easily than AlN in high-manganese steel. Calculations for oxide inclusions in high-manganese steel are not available because of the lack of physical properties. The measurement of the contact angle and interfacial energy between the inclusion and liquid steel could assist in developing a comprehensive understanding of inclusion agglomeration behavior in different steel grades.

ACKNOWLEDGEMENTS

The authors thank the Natural Sciences and Engineering Research Council of Canada (NSERC), the Canada Foundation for Innovation John Evans Leaders Fund (CFI JELF, Project No. 32826), and the McMaster Steel Research Centre (SRC) members for funding the research.

REFERENCES

1. L. Zhang and B.G. Thomas, *ISIJ Int.* 43, 271 (2003).
2. T.A. Engh, *Principles of Metals Refining* (New York: Oxford University Press, 1992), pp. 1–3.
3. L. Zhang and B.G. Thomas, *Metall. Mater. Trans. B* 37B, 733 (2006).
4. O. Wijk: Inclusion engineering, in *Proc. 7th Int. Conf. Refining Process* (SCANINJECT 733. VII), Luleå, Sweden (1995), p. 35.
5. H. Chikama, H. Shibata, T. Emi, and M. Suzuki, Mater. Trans. *JIM* 37, 620 (1996).
6. H. Shibata, H.B. Yin, S. Yoshinaga, T. Emi, and M. Suzuki, *ISIJ Int.* 38, 149 (1998).
7. W. Mu, H. Shibata, P. Hedström, P.G. Jönsson, and K. Nakajima, *Steel Res. Int.* 87, 10 (2016).
8. W. Mu, P.G. Jönsson, and K. Nakajima, *J. Mater. Sci.* 51, 2168 (2016).
9. H.B. Yin, H. Shibata, T. Emi, and M. Suzuki, *ISIJ Int.* 37, 936 (1997).
10. H.B. Yin, H. Shibata, T. Emi, and M. Suzuki, *ISIJ Int.* 37, 946 (1997).
11. K. Nakajima and S. Mizoguchi, *Metall. Mater. Trans. B* 32, 629 (2001).
12. S. Kimura, K. Nakajima, and S. Mizoguchi, *Metall. Mater. Trans. B* 32, 79 (2001).
13. W. Mu, N. Dogan, and K.S. Coley, *Metall. Mater. Trans. B* 48, 2379 (2017).
14. W. Mu, N. Dogan, and K.S. Coley, *Metall. Mater. Trans. B* 48, 2092 (2017).
15. W. Mu, N. Dogan, and K.S. Coley, *J. Mater. Sci.* (2018). https://doi.org/10.1007/s10853-018-2268-6.
16. B. Coletti, B. Blanpain, S. Vantilt, and S. Sridhar, *Metall. Mater. Trans. B* 34, 533 (2003).
17. S. Vantilt, B. Coletti, B. Blanpain, J. Fransaer, P. Wollants, and S. Sridhar, *ISIJ Int.* 44, 1 (2004).
18. G. Liang, C. Wang, and Y. Fang, *Acta Metall. Sin. Chin. Ed.* 42, 708 (2006).
19. J. Appelberg, K. Nakajima, H. Shibata, A. Tilliander, and P. Jönsson, *Mater. Sci. Eng. A* 495, 330 (2008).
20. Y. Kang, B. Sahebkar, P.R. Scheller, K. Morita, and D. Sichen, *Metall. Mater. Trans. B* 42, 522 (2011).
21. G. Du, J. Li, Z.B. Wang, and C.B. Shi, *Steel Res. Int.* 88, 1600185 (2016). https://doi.org/10.1002/srin.201600185.
22. S.K. Michelic, U.D. Salgado, C. Bernhard, and I.O.P. Conf, Series. *Mater. Sci. Eng.* 143, 012010 (2016).
23. J. Wikström, K. Nakajima, H. Shibata, A. Tilliander, and P. Jönsson, *Ironmak Steelmak* 35, 589 (2008).
24. P. Misra, V. Chevrier, S. Sridhar, and A. Cramb, *Metall. Mater. Trans. B* 31, 1135 (2000).
25. P. Misra, S. Sridhar, and A. Cramb, *Metall. Mater. Trans. B* 32, 963 (2001).
26. J. Wikström, K. Nakajima, H. Shibata, A. Tilliander, and P. Jönsson, *Mater. Sci. Eng. A* 495, 316 (2008).
27. P.A. Kralchevsky, V.N. Paunov, N.D. Denkov, I.B.V. Ivanoc, and K. Nagayama, *J. Colloid. Interface Sci.* 155, 420 (1993).
28. V.N. Paunov, P.A. Kralchevsky, N.D. Denkov, and K. Nagayama, *J. Colloid. Interface Sci.* 157, 100 (1993).
29. S.C. Lee, C. Tse, K.W. Yi, P. Misra, V. Chevrier, C. Orrling, S. Sridhar, and A. Cramb, *J. Non-Cryst. Solids* 282, 41 (2001).
30. K. Miao, A. Haas, M. Sharma, W. Mu, and N. Dogan, *Metall. Mater. Trans. B* (2017, Unpublished work).
31. B.J. Monaghan and L. Chen, *J. Non-Cryst. Solids* 347, 254 (2004).
32. B.J. Monaghan and L. Chen, *Ironmak Steelmak* 33, 323 (2006).
33. B.J. Monaghan, L. Chen, and J. Sorbe, *Ironmak Steelmak* 32, 258 (2005).
34. S. Feichtinger, S.K. Michelic, Y.B. Kang, and C. Bernhard, *J. Am. Ceram. Soc.* 97, 316 (2014).
35. E. Jahnke, F. Emde, and F. Lösch, *Tables of Higher Functions* (New York: McGraw-Hill, 1960).
36. M. Abramovitz and I.A. Stegun, *Handbook of Mathematical Functions* (New York: Dover, 1965).
37. C.F. Chan Man Fong, D. De Kee, and P.N. Kaloni, *Advanced Mathematics for Engineering and Science* (Singapore: World Scientific Publishing Co. Pte. Ltd., 2003), p. 5.
38. Y.N. Wang, J. Yang, X.L. Xin, R.Z. Wang, and L.Y. Xu, *Metall. Mater. Trans. B* 47, 1378 (2016). https://doi.org/10.1007/s11663-015-0568-7.
39. J. Yang, Y.N. Wang, X.M. Ruan, R.Z. Wang, K. Zhu, Z.J. Fan, Y.C. Wang, C.B. Li, and X.F. Jiang, *Metall. Mater. Trans. B* 46, 1365 (2015).
40. J.H. Park, D.-J. Kim, and D.J. Min, *Metall. Mater. Trans. A* 43, 2316 (2012).
41. N. Kikuchi, S. Nabeshima, Y. Kishimoto, T. Matsushita, and S. Sridhar, *ISIJ Int.* 47, 1255 (2007).
42. J.F. Lynch, C.G. Ruderer, and W.H. Duckworth, *Engineering Properties of Selected Ceramic Materials* (Columbus, OH: American Ceramic Society, Inc., 1966).
43. B.J. Keene, Contact angle and work of adhesion between ferrous melts and non-metallic solid, Slag Atlas (2nd edn), ed. by Verein Deutsscher Eisenhüttenleute (VDEh) (Verlag Stahleisen GmbH, 1995), pp. 513–539.
44. B.J. Keene and K.C. Mills, Densities of molten slag, Slag Atlas (2nd edn), ed. by Verein Deutsscher Eisenhüttenleute (VDEh) (Verlag Stahleisen GmbH, 1995), pp. 313–347.
45. G.S. Ershov and A.M. Kovalenko, *Russ. Metall.* 1, 47 (1968).
46. C.V. Ciobanu, D.T. Tambe, and V.B. Shenoy, *Surf. Sci.* 582, 145 (2005).
47. S.K. Rhee, *J. Am. Ceram. Soc.* 53, 639 (1970).